Mefloquine, a Potent Anti-severe Acute Respiratory Syndrome-Related Coronavirus 2 (SARS-CoV-2) Drug as an Entry Inhibitor *in vitro*

Kaho Shionoya[1,2], Masako Yamasaki[1,2], Shoya Iwanami[3,4], Yusuke Ito[4], Shuetsu Fukushi[5], Hirofumi Ohashi[1,2], Wakana Saso[1,6,7], Tomohiro Tanaka[8], Shin Aoki[9], Kouji Kuramochi[2], Shingo Iwami[3,4,10,11,12,13,14], Yoshimasa Takahashi[15,16], Tadaki Suzuki[17], Masamichi Muramatsu[1], Makoto Takeda[18], Takaji Wakita[1] and Koichi Watashi[1,2,10,16,19]*

[1] Department of Virology II, National Institute of Infectious Diseases, Tokyo, Japan, [2] Department of Applied Biological Science, Tokyo University of Science, Tokyo, Japan, [3] Interdisciplinary Biology Laboratory (iBLab), Division of Biological Science, Graduate School of Science, Nagoya University, Nagoya, Japan, [4] Department of Biology, Faculty of Sciences, Kyushu University, Fukuoka, Japan, [5] Department of Virology I, National Institute of Infectious Diseases, Tokyo, Japan, [6] The Institute of Medical Science, The University of Tokyo, Tokyo, Japan, [7] AIDS Research Center, National Institute of Infectious Diseases, Tokyo, Japan, [8] Faculty of Pharmaceutical Sciences, Tokyo University of Science, Tokyo, Japan, [9] Research Institute for Science and Technology, Tokyo University of Science, Tokyo, Japan, [10] MIRAI, JST, Saitama, Japan, [11] Institute of Mathematics for Industry, Kyushu University, Fukuoka, Japan, [12] Institute for the Advanced Study of Human Biology (ASHBi), Kyoto University, Kyoto, Japan, [13] NEXT-Ganken Program, Japanese Foundation for Cancer Research (JFCR), Tokyo, Japan, [14] Science Groove Inc., Fukuoka, Japan, [15] Department of Immunology, National Institute of Infectious Diseases, Tokyo, Japan, [16] Research Center for Drug and Vaccine Development, National Institute of Infectious Diseases, Tokyo, Japan, [17] Department of Pathology, National Institute of Infectious Diseases, Tokyo, Japan, [18] Department of Virology III, National Institute of Infectious Diseases, Tokyo, Japan, [19] Institute for Frontier Life and Medical Sciences, Kyoto University, Kyoto, Japan

Coronavirus disease 2019 (COVID-19) has caused serious public health, social, and economic damage worldwide and effective drugs that prevent or cure COVID-19 are urgently needed. Approved drugs including Hydroxychloroquine, Remdesivir or Interferon were reported to inhibit the infection or propagation of severe acute respiratory syndrome-related coronavirus 2 (SARS-CoV-2), however, their clinical efficacies have not yet been well demonstrated. To identify drugs with higher antiviral potency, we screened approved anti-parasitic/anti-protozoal drugs and identified an anti-malarial drug, Mefloquine, which showed the highest anti-SARS-CoV-2 activity among the tested compounds. Mefloquine showed higher anti-SARS-CoV-2 activity than Hydroxychloroquine in VeroE6/TMPRSS2 and Calu-3 cells, with IC_{50} = 1.28 μM, IC_{90} = 2.31 μM, and IC_{99} = 4.39 μM in VeroE6/TMPRSS2 cells. Mefloquine inhibited viral entry after viral attachment to the target cell. Combined treatment with Mefloquine and Nelfinavir, a replication inhibitor, showed synergistic antiviral activity. Our mathematical modeling based on the drug concentration in the lung predicted that Mefloquine administration at a standard treatment dosage could decline viral dynamics in patients, reduce cumulative viral load to 7% and shorten the time until virus elimination by 6.1 days. These data cumulatively underscore Mefloquine as an anti-SARS-CoV-2 entry inhibitor.

Keywords: COVID-19, severe acute respiratory syndrome-related coronavirus 2, SARS-CoV-2, repurposing, malaria, mefloquine, coronavirus

INTRODUCTION

Coronavirus disease 2019 (COVID-19), caused by infection of severe acute respiratory syndrome-related coronavirus 2 (SARS-CoV-2), has spread into a worldwide since it was first reported in Wuhan, China in December 2019, and caused severe damage to public health, the economy, and society in many countries and areas. Several therapeutic drug candidates, including Remdesivir (RDV), Hydroxychloroquine (HCQ), Lopinavir and Interferon, have been undergone clinical trials with drug-repurposing approaches (Touret et al., 2020), of which treatment efficacies have yet been fully demonstrated. New drug choices for both therapeutic and prophylactic use against COVID-19 are urgent needs.

Chloroquine and its derivative, HCQ, are used clinically as anti-malarial drugs (Sinha et al., 2014). These drugs (particularly the less toxic HCQ) were expected to be COVID-19 drug candidates from the early days of the COVID-19 pandemic (Cortegiani et al., 2020), given their anti-SARS-CoV-2 activity *in vitro* and the ability to reduce pathogenesis caused by the related coronaviruses, SARS-CoV and human coronavirus OC43 *in vivo* (Keyaerts et al., 2009; Liu et al., 2020; Wang et al., 2020; Weston et al., 2020). However, despite over 30 randomized controlled trials or observational studies in different countries, no consensus demonstrates a sufficient anti-COVID-19 effect of these drugs (Geleris et al., 2020; Rosenberg et al., 2020; Tang et al., 2020; Yu B. et al., 2020). Therefore, the FDA revoked the emergency use of chloroquine and HCQ for COVID-19 treatment in June 2020. The discrepancy between *in vitro* and *in vivo* experimental data and the clinical outcomes reported to date is not well understood. Possibilities include differences in drug sensitivities among cell types used in experiments (see section "Discussion") and the insufficient potential of anti-SARS-CoV-2 activity of these drugs: The concentrations of HCQ required for 50 and 90% virus reduction (IC_{50}, IC_{90}), determined *in vitro* (i.e., several µM), is higher than an achievable in plasma value in clinical settings (1–2 µM at the maximum) (McLachlan et al., 1993; Hattori et al., 2020; Liu et al., 2020; Touret et al., 2020) (see section "Discussion"). Thus, identifying another drug with a higher antiviral potential at the maximum drug concentration based on clinical data is a probable approach to improving the treatment efficacy.

In this study, from a cell-based functional screening of FDA/EMA/PMDA-approved anti-parasitic/anti-protozoal drugs, we identified Mefloquine (MFQ), a derivative of HCQ originally used for anti-malarial therapy and prophylaxis (Sinha et al., 2014), that has a higher anti-SARS-CoV-2 activity than HCQ in both tansmembrane protease, serine 2 gene (TMPRSS2)-overexpressed VeroE6 cells and human lung-derived Calu-3 cells. MFQ inhibited viral entry process after attachment of the virus to the cell. Importantly, our mathematical modeling predicted that MFQ administration (1,000 mg, once) could decline viral dynamics in patients to significantly reducing the cumulative viral load and shortening the period until virus elimination in clinical concentration ranges. Our data provide foundational evidence that proposes MFQ as an alternative drug for anti-COVID-19 treatment.

MATERIALS AND METHODS

Cell Culture

VeroE6/TMPRSS2 cells, a VeroE6 cell clone overexpressing the TMPRSS2 from Japanese Collection of Research Bioresources (JCRB) cell bank (Nao et al., 2019; Matsuyama et al., 2020), were cultured in Dulbecco's modified Eagle's medium (D-MEM; Wako) supplemented with 10% fetal bovine serum (FBS; SIGMA), 100 units/mL penicillin, 100 µg/mL streptomycin, 10 mM HEPES (pH 7.4) and 1 mg/mL G418 (Nacalai) at 37°C in 5% CO_2. During the infection assay, G418 was removed and 10% FBS was replaced with 2% FBS. Calu-3 cells, a human lung epithelial cell line, were cultured in the above medium without G418 through the assay. Human hepatoma cell line, Huh-7 cells, were cultured in D-MEM supplemented with 10% FBS (SIGMA), 100 units/mL penicillin, 100 µg/mL streptomycin, 10 mM HEPEPS (pH 7.4), 0.1 mM nonessential amino acids (Invitrogen) and 1 mM sodium pyruvate.

Reagents

All the reagents were purchased from ChemScene, Selleck, Cayman Chemical, Tokyo Chemical Industry (TCI), Sigma and Mochida pharmaceutical cooperation.

Infection Assay

SARS-CoV-2 was handled in a biosafety level 3 (BSL3) facility. We used the SARS-CoV-2 Wk-521 strain, a clinical isolate from a COVID-19 patient, that was propagated in VeroE6/TMPRSS2 cells and amplified (Matsuyama et al., 2020). Virus infectious titer ($TCID_{50}$/mL) was measured by observing the cytopathic effect of cells inoculated with 10-fold serial dilution of the virus (Matsuyama et al., 2020). For the infection assay using VeroE6/TMPRSS2 cells, SARS-CoV-2 was inoculated at a multiplicity of infection (MOI) of 0.001 for 1 h, and the unbound virus was removed by washing (**Figures 1B–E**, **2B**, **3B,C**, **4A**, left). Cells were cultured for 24 h to measure extracellular viral RNA or to detect viral N protein, or for 48 h to observe virus-induced cytopathic effect (CPE). Compounds were added during virus inoculation (1 h) and after inoculation (24 or 48 h), except the time-of-addition assay (**Figure 3B**) and the assay evaluating the post-attachment phase from membrane fusion to virus secretion (**Figure 3D**).

The Calu-3 cell infection assay was performed by virus inoculation [100 (**Figure 1F**) and 1,000 (**Supplementary Figure 2A**) times higher amount of virus inoculation compared with that in VeroE6/TMPRSS2-based assay] for 3 h and incubation for an additional 72 h to detect viral N protein (**Figure 1F**) or quantify viral RNA in the culture supernatant (**Supplementary Figure 2A**).

Compound Screening

We screened 27 approved anti-parasitic and anti-protozoal drugs (Selleck). VeroE6/TMPRSS2 cells were treated with 5 µM of each drug for 1 h during virus inoculation at an MOI of 0.001. After removing the unbound virus, the cells were incubated with the drugs for an additional 48 h and were
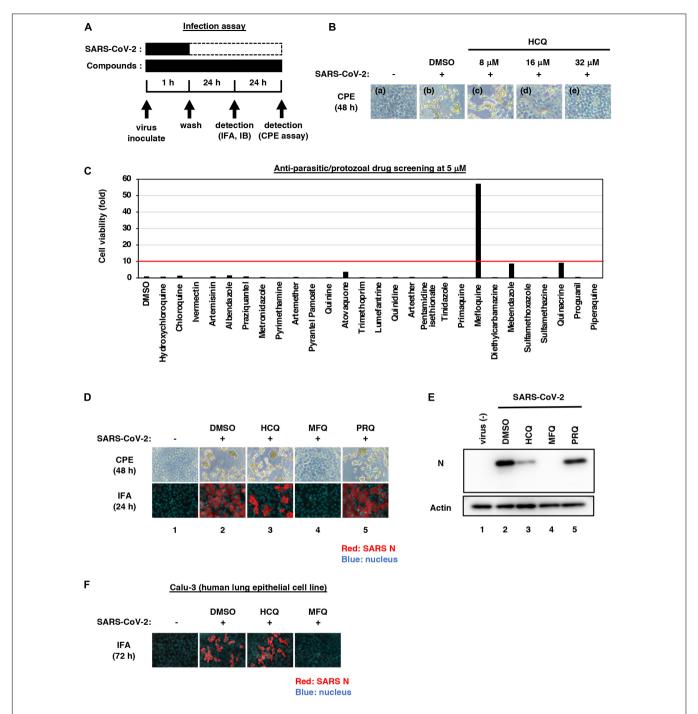
FIGURE 1 | Mefloquine (MFQ) inhibits Severe Acute Respiratory Syndrome-related coronavirus 2 (SARS-CoV-2) propagation. **(A)** Schematic representation of the SARS-CoV-2 infection assay. VeroE6/TMPRSS2 cells were inoculated with SARS-CoV-2 (Wk-521 strain) at an MOI of 0.001 for 1 h. After removing the unbound virus, cells were cultured for 24 h to detect virus-encoding N protein by immunofluorescence assay (IFA) and immunoblot (IB) or to detect viral RNA in the culture supernatant by RT-qPCR, or for 48 h to observe virus-induced cytopathic effect (CPE). Compounds were treated given throughout the assay. **(B)** Dose dependency of Hydroxychloroquine (HCQ) on CPE suppression. VeroE6/TMPRSS2 cells were inoculated with the virus for 1 h. Removing the unbound virus, cells were cultured with a medium containing the indicated compounds for 48 h. CPE was observed by microscopy. **(C)** Screening of anti-parasitic/protozoal drugs in the cell-based infection assay. Compounds were administrated at 5 μM, at which hydroxychloroquine showed little effect on CPE. The viability of infected cells was quantified via a high content imaging analyzer by setting the value for the sample treated with DMSO solvent as 1. MFQ showed more than 57-fold higher cell viability than DMSO controls. **(D,E)** SARS-CoV-2-induced CPE and viral N protein expression upon compound treatments [DMSO at 0.08%; hydroxychloroquine (HCQ), mefloquine (MFQ), and primaquine (PRQ) at 8 μM]. Red and blue signals of merged images indicate viral N protein and nucleus, respectively (**D**, lower). Viral N protein and actin, an internal control, were detected by immunoblot **(E)**. **(F)** The anti-SARS-CoV-2 activity of the indicated compounds in Calu-3 cells, a human lung epithelial cell-derived line.

recovered, fixed in 4% paraformaldehyde and stained with 0.02% 4′,6-diamidino-2-phenylindole (DAPI). The number of surviving cells was quantified with a high content imaging analyzer. The survival cell numbers treated with each drug are presented as a fold value relative to the cells treated with DMSO solvent (**Figure 1C** and **Supplementary Figure 1**). Drugs that protected cells from virus-induced CPE to more than 10-fold of the infected cells treated with DMSO were selected as hits.

Immunofluorescence and Immunoblot Analysis

Viral encoded N protein expression was detected using a rabbit anti-SARS-CoV N antibody (Mizutani et al., 2004) as a primary antibody with anti-rabbit AlexaFlour 568 or anti-rabbit IgG-HRP (Thermo Fisher Scientific) as a secondary antibody by indirect immunofluorescence or immunoblot analysis (**Figures 1D–F**) as previously reported (Ohashi et al., 2018). Anti-actin (Sigma) was used as an internal control for the immunoblot analysis. For immunofluorescence, nuclei were stained with DAPI (blue).

Quantification of Viral RNA

Viral RNA was extracted with QIAamp Viral RNA Mini Kit (QIAGEN), RNeasy Mini Kit (QIAGEN) and MagMAX^{TM} Viral/Pathogen II Nucleic Acid Isolation Kit (Thermo Fisher Scientific). We quantified viral RNA by real time RT-PCR analysis with a one-step RT-qPCR kit (THUNDERBIRD Probe One-step RT-qPCR kit, TOYOBO) using 5′-ACAGGTACGTTAATAGTTAATAGCGT-3′ for forward primer and 5′-ATATTGCAGCAGTACGCACACA-3′ for reverse primer, and a 5′-FAM-ACACTAGCCATCCTTACTGCGCTTCG-3′ probe, as described (Corman et al., 2020). The detection limit of SARS-CoV-2 RNA in this study was 39 cycle (C_t value).

Cell Viability

Cell viability was examined by MTT assay as previously reported (Ohashi et al., 2018; **Figure 2C**) or by quantification of survival cell numbers fixed with 4% paraformaldehyde and stained with 0.02% DAPI with a high content imaging analyzer ImageXpress Micro Confocal (MOLECULAR DEVICES) (**Figures 1C, 4A**, right and **Supplementary Figure 2B**).

Time-of-Addition Analysis

VeroE6/TMPRSS2 cells were inoculated with the virus at an MOI of 0.001 for 1 h, and the free virus was removed by washing. Compounds were added at three different times before measuring extracellular viral RNA (**Figure 3B**): (a) throughout the entire assay covering viral lifecycle (whole: 1 h + 24 h after virus inoculation), (b) only the early phase of the assay covering viral entry steps (entry: initial 1 h + 2 h after virus inoculation), (c) during the late phase of the assay, from viral replication to viral secretion (post-entry: last 22 h after virus inoculation).

Virus-Cell Attachment Assay

Virus and compounds were preincubated at 4°C for 1 h and then exposed to VeroE6/TMPRSS2 cells at 4°C for 5 min to allow virus-cell attachment. After removing unbound virus by washing, attached viral RNA was extracted with RNeasy Mini Kit (QIAGEN) and measured by real time RT-qPCR. The same assay was done without cells to measure the background level. Heparin was used as a positive control that inhibits SARS-CoV-2 attachment to cells. The specific cell-attached SARS-CoV2 RNA was calculated by subtracting viral RNA levels without cells from those with VeroE6/TMPRSS2 cells and are shown in **Figure 3C**.

Post-attachment Assay

The assay examining the steps from Spike cleavage/membrane fusion through viral secretion, was conducted by initiating compound treatment after viral attachment to already highly infected cells and detecting the secreted virus for a short duration (**Figure 3D**): Cells were incubated with the virus at an MOI of 1.5 at 4°C for 1 h, then removing the unattached virus. These virus-attached cells were incubated at 37°C for 6 h in the presence of compounds to allow viral entry through replication and secretion. The culture supernatant was recovered to detect extracellular viral RNA. E-64d (12.5 μM), lysosomal/cytosolic cysteine protease inhibitor, was used as a positive control.
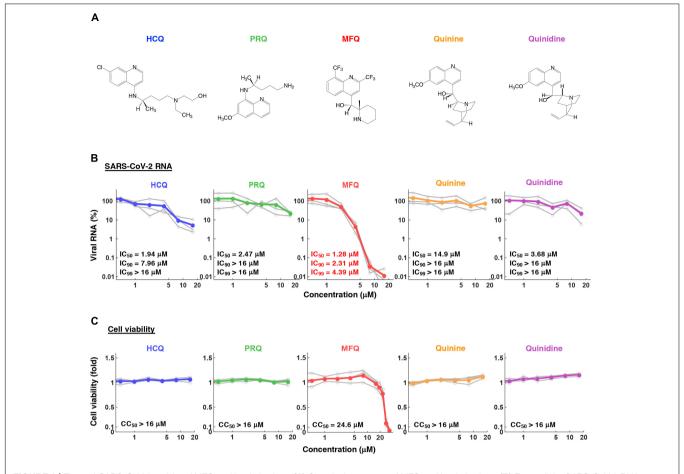
Pseudovirus Infection Assay

SARS-CoV-2 pseudotype virus was produced using the vesicular stomatitis virus (VSV)-pseudotype system essentially as described previously (Fukushi et al., 2005; Tani et al., 2010) using the expression plasmid encoding the SARS-CoV-2 Spike protein and G-deficient VSV, which contains the luciferase gene instead of the VSV-G gene. HCV pseudotype virus was prepared from the retrovirus pseudoparticle system using the expression plasmid for murine leukemia virus Gag-Pol, luciferase protein and HCV E1E2 envelope protein (kindly provided by Dr. Francois-Loic Cosset at University of Lyon) as described (Bartosch et al., 2003).

The pseudovirus for SARS-CoV-2 was inoculated to VeroE6/TMPRSS2 cells in the presence or absence of compounds and the intracellular luciferase activity was measured at 24 h post-inoculation. Camostat (TCI) 50 μM and E-64d (Cayman) 50 μM were used as a positive control to inhibit SARS-CoV-2 entry (**Figure 3E**, left). HCV pseudotype virus was inoculated to Huh-7 cells (kindly provided by Dr. Francis Chisari at The Scripps Research Institute) for 4 h, followed by washing, culturing for 72 h and measuring luciferase activity. Compounds were treated for 1 h prior to infection and for 4 h during the virus inoculation. Bafilomycin A1 at 10 nM was used as a positive control for inhibiting HCV entry (**Figure 3E**, right).

Statistical Analysis

Statistical significance was analyzed using the two-tailed Student's t-test ($^*p < 0.05$; $^{**}p < 0.01$; N.S., not significant).

FIGURE 2 | The anti-SARS-CoV-2 activity of MFQ and its derivatives. **(A)** Chemical structures of MFQ and its derivatives. **(B)** Extracellular SARS-CoV-2 RNA was quantified upon treatment with HCQ, MFQ and related compounds PRQ, Quinine and Quinidine at varying concentrations. Calculated inhibitory concentrations of 50, 90, and 99% maximum (IC_{50}, IC_{90}, and IC_{99}) for each compound are as indicated. **(C)** Cell viability was measured by MTT assay with the calculated 50% maximal cytotoxic concentration (CC_{50}).

RESULTS

Identification of Mefloquine as a Potential Inhibitor Against SARS-CoV-2 Infection

In this study, we mainly used VeroE6/TMPRSS2 cells, which is established by overexpressing transmembrane serine protease 2 (TMPRSS2) in VeroE6 cells (Nao et al., 2019; Matsuyama et al., 2020), and human lung epithelial-derived Calu-3 cells in a part of experiments, as SARS-CoV-2 infection models. First, we examined the dose dependency of HCQ for antiviral activity by a cytopathic effect (CPE) assay: VeroE6/TMPRSS2 cells were inoculated with SARS-CoV-2 at an MOI of 0.001 for 1 h, washed to remove unbound virus, and incubated for an additional 48 h (**Figure 1A**). SARS-CoV-2 propagation in the cells exhibited an intensive cytopathic effect (**Figure 1B**, panel b), as reported (Matsuyama et al., 2020). HCQ protected cells from SARS-CoV-2-induced cytopathology completely at the concentration of 32 μM, remarkably but not completely at 16 μM, and very little at 8 μM (**Figure 1B**, panels c–e).

Aiming to identify drugs with greater anti-SARS-CoV-2 potential than HCQ, we employed 5 μM for drug screening, a concentration at which HCQ had no CPE suppression. As a drug library, we used approved anti-parasitic/anti-protozoal drugs for following two reasons; (1) In addition to Chloroquine and HCQ, some drugs such as Ivermectin, Atovaquone, and quinoline derivatives were reported to demonstrate antiviral activities against other RNA viruses (Mastrangelo et al., 2012; Al-Bari, 2015; Cifuentes Kottkamp et al., 2019; DeWald et al., 2019). (2) Anti-parasitic/anti-protozoal agents generally reach high concentrations (i.e., over μM ranges) in the plasma in clinical settings (Sinha et al., 2014). We thus screened 27 FDA/EMA/PMDA-approved (or approved in the past) anti-parasitic/anti-protozoal drugs at 5 μM by the CPE assay (**Figure 1C** and **Supplementary Figure 1**). By following the scheme shown in **Figure 1A**, cells at 48 h post-inoculation were fixed, stained with DAPI, and counted to quantify survival cell numbers. The graph in **Figure 1C** shows survival cell numbers relative to that of DMSO-treated cells as a control, and survival cell number relative to that of non-infected cells are shown in **Supplementary Figure 1**. In this screening,
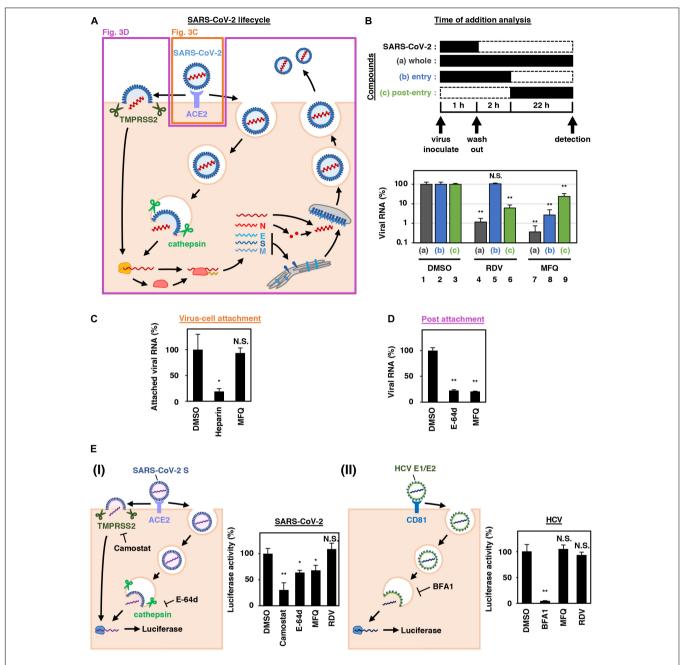
FIGURE 3 | MFQ inhibits the SARS-CoV-2 entry process. **(A)** SARS-CoV-2 life cycle. SARS-CoV-2 infection is initiated with virus attachment to the host cells that involves the cellular receptor, angiotensin converting enzyme 2 (ACE2), followed by the cleavage of viral Spike (S) proteins by either transmembrane serine protease (TMPRSS2) on the plasma membrane or cathepsins in the endosome/lysosome that induces fusion of viral and host membranes. Viral RNA is translated, processed and replicated to be assembled into progeny virus with viral structural proteins and released extracellularly. **(B)** Scheme of the time of addition analysis. Compounds were treated at three different times: **(a)** whole: throughout the assay for 25 h, **(b)** entry: for the initial 3 h to evaluate the effect on the viral entry process and **(c)** post-entry: for the last 22 h to evaluate the effect on viral replication/re-infection. Viral RNA levels in the culture supernatant are shown in the graph by setting that upon DMSO treatment as 100%. **(C)** Virus-cell attachment assay. VeroE6/TMPRSS2 cells were exposed to virus at an MOI of 0.001 at 4°C for 5 min with 50 μM MFQ or 100 U/mL Heparin, a SARS-CoV-2 attachment inhibitor used as a positive control. After washing the unbound virus, cell surface-attached virus was extracted and quantified by real-time RT-PCR. **(D)** Post-attachment assay. For evaluating the activity after virus attachment, from membrane fusion to virus secretion, VeroE6/TMPRSS2 cells preincubated with the virus at an MOI of 1.5 at 4°C for 1 h to allow virus attachment were treated with compounds for 6 h at 37°C. Extracellular viral RNA was quantified by RT-qPCR. E-64d, a cysteine protease inhibitor, was used as a positive control. **(E)** Pseudovirus assays carrying the SARS-CoV-2 Spike or hepatitis C virus (HCV) E1E2 envelope. In the SARS-CoV-2 pseudovirus assay, Camostat and E-64d were used as positive controls for inhibiting TMPRSS2 and cysteine protease, respectively **(E**, left). Bafilomycin A1 (BFA1), which reported to inhibit HCV entry, was used as a positive control for HCV pseudovirus assay **(E**, right). $*p < 0.05$ and $**p < 0.01$.
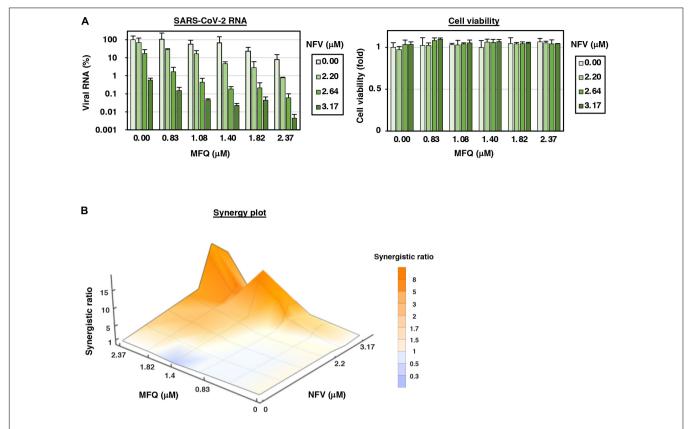
FIGURE 4 | MFQ shows synergistic anti-SARS-CoV2 activity with replication inhibitor NFV. **(A)** Viral RNAs in the culture supernatant at 24 h after co-treatment with MFQ and NFV were quantified by real-time RT-PCR. Relative values are shown of viral RNA or cell viability to those treated with DMSO control. Cell viability was simultaneously measured with a high content image analyzer. [MFQ at 0, 0.83, 1.08, 1.40, 1.82, and 2.37 μM (1.3-fold-dilution); NFV at 0, 2.20, 2.64, and 3.17 μM (1.2-fold-dilution)]. **(B)** The three-dimensional interaction landscapes of NFV and MFQ were evaluated with the Bliss independence model. Orange, white and dark-blue colors on the contour plot indicate synergy, additive and antagonism, respectively.

HCQ, Chloroquine and Ivermectin had little effect, while MFQ remarkably protected cells from the virus-induced CPE, with a more than 57-fold increase in surviving cells over those of the vehicle control (**Figure 1C**).

We next compared the antiviral activities of MFQ with that of HCQ and an additional Chloroquine derivative, Primaquine (PRQ), as a reference. Cytopathogenicities at 48 h and the viral N protein expression at 24 h after virus inoculation (a time before showing CPE) were examined during treatment with each compound at 8 μM (**Figures 1D,E**): MFQ completely protected cells from viral propagation-induced CPE and reduced the production of viral protein (lane 4), whereas HCQ weakly exerted an antiviral effect (lane 3), and PRQ had little antiviral effect (lane 5). To examine whether the observed antiviral effects depend on cell types or are generally reproduced beyond cell types, we used a human lung epithelial cell line, Calu-3, and found the robust antiviral activity of MFQ against SARS-CoV-2, in contrast to much lower HCQ activity (**Figure 1F**). Therefore, we focused on MFQ as a potential anti-SARS-CoV-2 drug in subsequent analyses.

Antiviral Profile of Mefloquine and Other Quinoline Derivatives

To profile the anti-SARS-CoV-2 activity of compounds, we quantified viral RNA released into the culture supernatant in addition to cell viability at 24 h after virus inoculation upon treatment at varying concentrations (0.5, 1, 2, 4, 8, and 16 μM) of HCQ, PRQ, MFQ, and other related compounds, Quinine and Quinidine, that possess a quinoline ring (**Figures 2A–C**). The 50, 90, and 99% maximal inhibitory concentrations (IC_{50}, IC_{90}, and IC_{99}) and 50% maximal cytotoxic concentrations (CC_{50}) are shown. HCQ and MFQ demonstrated antiviral activities in a dose-dependent manner, with higher potency for MFQ than HCQ (**Figure 2B**). By contrast, PRQ showed marginal antiviral effects at all concentrations examined (see section "Discussion" for structural implication). We also confirmed the effect of MFQ on SARS-CoV-2 RNA and the cell viability in Calu-3 cells (**Supplementary Figure 2**), showing the consistent anti-SARS-CoV-2 activity at concentration ranges without cytotoxic effects.

Mefloquine Inhibits the SARS-CoV-2 Entry Process After Virus-Cell Attachment

SARS-CoV-2 attaches to target cells by the binding of viral Spike protein to its receptor, angiotensin-converting enzyme 2 (ACE2). It is then subjected to Spike cleavage by host proteases, either TMPRSS2 on the plasma membrane or cathepsins in the endosomes, followed by the membrane fusion and the sorting to the site of replication (entry phase). Viral RNA then replicates and assembles with viral structural proteins to produce progeny virus (replication phase) (**Figure 3A**; Hoffmann et al., 2020; Lebeau et al., 2020).

We next addressed which step in the viral life cycle MFQ inhibits by a series of assays. The time-of-addition analysis, in which compounds are treated at different times, is used to evaluate the phase of viral entry and replication separately (Wang et al., 2020). As previously reported (Wang et al., 2020), compounds were treated at three different time points (**Figure 3B**), either throughout the assay (a; whole life cycle, 1 h during virus inoculation + 24 h after inoculation), for the initial 3 h (b; entry phase, 1 h during virus inoculation + 2 h after inoculation), or for the last 22 h (c; post-entry phase, including replication). In this analysis, RDV, a reported replication inhibitor (Wang et al., 2020), had no inhibitory effect when applied during the initial 3 h (**Figure 3B**, lane 5), but it decreased viral RNA in the post-entry phase (**Figure 3B**, lane 6). By contrast, MFQ remarkably reduced viral RNA levels to under 3% when applied at the entry phase (**Figure 3B**, lane 8), but showed much lower antiviral activity (to 24%) when treated after the first round of viral entry (**Figure 3B**, lane 9). The viral RNA reduction by MFQ in lane 9 was likely to the inhibition of second round of infection and thereafter of the produced virus, which occurred during the 22 h. These data suggest that MFQ inhibits the entry process of SARS-CoV-2.

We then evaluated the virus-cell attachment in the presence or absence of MFQ by incubating cells with the virus at 4°C to allow viral attachment to the cell surface but not the following processes. After washing the unattached virus and compounds, we extracted and quantified the viral RNA on the cell surface. SARS-CoV-2 RNA from virus attached the surface of the cell was drastically reduced in the presence of heparin, an entry inhibitor for SARS-CoV-2, used as a positive control (Tandon et al., 2020; Tree et al., 2020), while that was not affected by MFQ treatment (**Figure 3C**). However, MFQ inhibited the post-attachment phase, ranging from the membrane fusion to virus production (**Figure 3D**): Virus-attached cells were prepared by incubation with a large amount of virus (MOI of 1.5, more than 1,000-fold higher than used in other normal infection assay) at 4°C for 1 h followed by washing. The cells were transferred to 37°C for 6 h in the presence or absence of compounds to induce membrane fusion and subsequent steps up to virus secretion, and viral RNA in the supernatant was quantified. MFQ clearly reduced the viral RNA levels to almost the same as those when treatment with E-64d, a lysosomal/cytosolic cysteine protease inhibitor reported to inhibited SARS-CoV-2 entry (Hoffmann et al., 2020; Hu et al., 2020; **Figure 3D**).

We further examined the virus entry using a pseudovirus carrying the Spike protein derived from SARS-CoV-2 or the envelope proteins of hepatitis C virus (HCV), another RNA virus unrelated to coronavirus (**Figure 3E**). These pseudoviruses can evaluate the entry mediated by these Spike or envelope proteins (Bartosch et al., 2003; Hoffmann et al., 2020). The pseudovirus assay showed that SARS-CoV-2 Spike-dependent viral entry was significantly inhibited by the TMPRSS2 inhibitor Camostat, and by MFQ to similar levels to those of E-64d (**Figure 3E**, left). However, the assay sensitivity itself was relatively lower than the SARS-CoV-2 infection assay. Meanwhile, HCV envelope-mediated entry was not affected by MFQ, in contrast to the reduced entry caused by Bafilomycin A1, a reported HCV entry inhibitor (**Figure 3E**, right). These results cumulatively suggest that MFQ inhibited the post-attachment SARS-CoV-2 Spike-dependent entry process.

Synergistic Antiviral Activity of Combined Treatment of Mefloquine With Nelfinavir

Combination treatment with multiple agents with different modes of action is a strategy to improve the outcome of antiviral treatments, including those against human immunodeficiency virus (HIV) and HCV (Shen et al., 2008; Koizumi et al., 2017). We, therefore, examined the combination of MFQ and a representative anti-SARS-CoV replication inhibitor, Nelfinavir (NFV) (Yamamoto et al., 2004). NFV has been suggested to inhibit SARS-CoV-2 replication thorough binding with the SARS-CoV-2 main protease by docking simulation (Ohashi et al., 2021). Following the experimental scheme in **Figure 1A**, we treated cells with paired compounds at varying concentrations for 24 h and quantified viral RNA in the cultured supernatant by real-time RT-PCR in addition to cell viability by a high content image analyzer. Viral RNA levels were reduced by a single treatment of either MFQ or NFV in a dose-dependent manner, and these was further reduced by combination treatment without any cytotoxicity (**Figure 4A**). Bliss independence-based synergy plot showed a synergistic antiviral effect in wide concentration ranges, especially at higher doses (**Figure 4B**, orange indicates synergistic effect).

Mathematical Prediction of the Mefloquine Treatment in Clinical Settings

Pharmacokinetics data for MFQ and HCQ, including the maximum drug concentration (C_{max}) in the plasma, half-life, and the distribution to the lung, are reported (Desjardins et al., 1979; Jones et al., 1994; Lim et al., 2009; Chhonker et al., 2018). Mathematical modeling combined with pharmacokinetics, pharmacodynamics, and the viral dynamics model described in section "Materials and Methods" (Ohashi et al., 2021) predicted the dynamics of viral load after MFQ (1,000 mg, once) and HCQ (400 mg, once per day) administration in patients (**Figure 5A**, red and blue, respectively) and the corresponding time-dependent antiviral activity of MFQ and HCQ (**Figure 5B**). The high antiviral potential and the long half-life of MFQ (more than 400 h) (Desjardins et al., 1979) were predicted to exert a
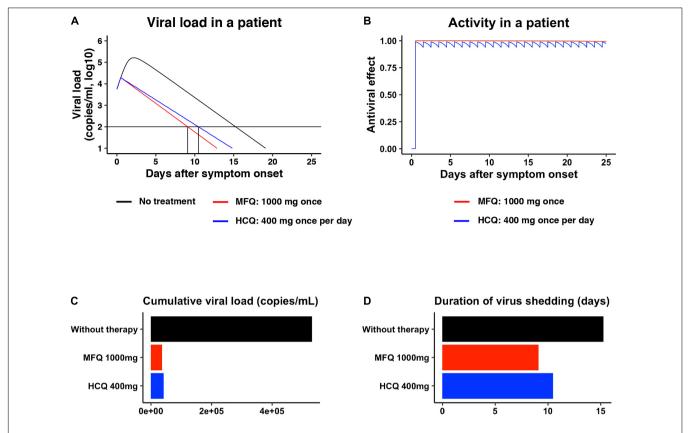
FIGURE 5 | Prediction of the impact of MFQ and HCQ treatment on SARS-CoV-2 dynamics in clinical settings. **(A,B)** The predicted viral load dynamics without (**A**, black), upon MFQ (1,000 mg oral, once) (**A**, red) or upon HCQ (400 mg oral, once per day) (**A**, blue) administration and the time-dependent antiviral activity of MFQ and HCQ **(B)** predicted by pharmacokinetics/pharmacodynamics/viral-dynamics (PK/PD/VD) models. **(C,D)** The cumulative viral load calculated as the area under the curve in **(A)** and the duration of virus shedding (days) [time from symptom onset to the day achieving a viral load under the detection limit (black horizontal line) in **(A)**] were evaluated for non-treatment (black), MFQ treatment (red) or HCQ treatment (blue).

continuous antiviral effect, and a resulting decline of viral load in a short period of time than HCQ (**Figure 5A**). Cumulative viral load, which is the area under the curve for the viral load over the time course, was calculated to be reduced by 6.98% in MFQ and 7.87% in HCQ, respectively (**Figure 5C**). The time until the viral load declines beneath the detectable level is 15.2 days without treatment, but it was calculated to be shortened to 10.5 days after HCQ treatment, whereas, 9.10 days after MFQ treatment (**Figure 5D**). These analyses predict the effectiveness of MFQ to reduce the viral load at clinical drug concentrations.

DISCUSSION

Given the *in vitro* anti-SARS-CoV-2 activity and the *in vivo* effect on the related coronaviruses (Ko et al., 2020; Liu et al., 2020; Wang et al., 2020; Weston et al., 2020), Chloroquine and HCQ have been expected to be effective as anti-COVID-19 drugs. However, accumulative data have not provided sufficient evidence supporting a preferable clinical outcome (Funnell et al., 2020). The IC_{50}, IC_{90}, and IC_{99} for HCQ calculated in this study were 1.94, 7.96, and 37.2 μM, respectively, consistent with the IC_{50} values at μM ranges examined in other studies (Gendrot et al., 2020; Hattori et al., 2020; Liu et al., 2020; Touret

et al., 2020). Pharmacokinetics analyses in healthy volunteers receiving oral administration of 200 mg HCQ demonstrated a C_{max} in the blood of 0.49–0.55 μM (McLachlan et al., 1993), lower than the concentration ranges having significant anti-SARS-CoV-2 activity. These data led us to identify a drug possessing a greater anti-SARS-CoV-2 potential. In this study, HCQ and MFQ demonstrated antiviral activities in a dose-dependent manner, with higher potency for MFQ than HCQ (**Figure 2B**). By contrast, PRQ showed marginal antiviral effects at all concentrations examined, suggesting that the hydroxyl and amino groups in the side chain of MFQ and/or that the position of the side chain on the quinoline ring are important for the anti-SARS-CoV-2 activity. The octanol-water partition coefficient (log P) values of MFQ, HCQ, Quinine, Quinidine and PRQ were calculated to be 4.34, 2.87, 2.48, 2.4, and 1.47, respectively (Ghose and Crippen, 1987), which imply that the higher hydrophobicity of MFQ, possibly due to the two trifluoromethyl groups, may contribute to its high antiviral activity. Furthermore, the antiviral effects might be associated with the electron density of the quinoline ring. MFQ, which has two strong electron-withdrawing trifluoromethyl groups in the quinoline ring, shows the strongest antiviral activity among the five analogs. HCQ, which has a moderate electron-withdrawing chlorine group, has moderate antiviral activity. PRQ, Quinine, and Quinidine, having the

electron-donating methoxy group (CH3O) into the quinoline ring, show decreased antiviral activities. Thus, the higher electron density of the quinoline ring might be related with the stronger antiviral effects against SARS-CoV-2.

SARS-CoV-2 entry requires the initial binding of the viral Spike protein to its cell surface receptor ACE2, then Spike cleavage by either of the two independent host proteases, endosomal pH-dependent cathepsin or plasma membrane pH-independent TMPRSS2 (Hoffmann et al., 2020; **Figure 3A**). Recently, it has been reported that the sensitivity to viral entry inhibitors such as Chloroquine, HCQ and a TMPRSS2 inhibitor Camostat depends on cell types, so that recommended not to rely only on widely used Vero cell line, but to use rather TMPRSS2-complemented Vero cells, Calu-3 cells or presumably primary respiratory/lung cell culture in an air-liquid interface system or organoids as a more physiologically relevant model for airway epithelial cells (Hoffmann et al., 2020; Suzuki et al., 2020). Due to the poor availability of primary cells, we employed VeroE6/TMPRSS2 and Calu-3 cells in this study, and discovered that MFQ inhibited the viral entry more potently than HCQ in these TMPRSS2-expressing cells. Importantly, standard MFQ treatment given to healthy volunteers achieved a plasma C_{max} of 4.58 μM with a long half-life (more than 400 h) (Karbwang and White, 1990), which is within concentration ranges exerting significant anti-SARS-CoV-2 activity *in vitro*. Moreover, it has been reported that the MFQ concentration in the lung was over 10-fold that of the blood in MFQ-treated human participants (Jones et al., 1994), expecting an even higher anti-SARS-CoV-2 effect of MFQ. Our mathematical model analysis (**Figure 5**) quantified this prediction, demonstrating a clear reduction in both cumulative viral load in patients and the time for viral elimination.

The *in vitro* anti-SARS-CoV-2 activity of MFQ itself has been reported (Fan et al., 2020; Gendrot et al., 2020; Jeon et al., 2020; Weston et al., 2020), however, they only reported the anti-SARS-CoV-2 activity in a single cell line (Vero or VeroE6 cells) with a single readout (viral RNA or CPE) at only one experimental condition without mechanistic analysis. In the present study, in addition to the comparing the activity of MFQ with HCQ and other analogs side-by-side, we characterized the modes of action and combination treatments. Furthermore, we addressed the clinical antiviral efficacy of MFQ by mathematical prediction, a significant scientific novelty. Our time-of-addition, virus-cell attachment, post attachment and pseudovirus assays suggest that MFQ inhibits the SARS-CoV-2 entry phase after attachment, including the viral Spike cleavage/membrane fusion and the following translocation to the replication complex. Detailed analysis of the mode of action is the object of future studies.

A limitation of our study is the use of antiviral profile data in cell culture assays but without an *in vivo* infection model. To date, SARS-CoV-2 studies have used models including hACE2-transgenic mice, ferrets, cats, hamsters, non-human primates and mice infected with mouse-adapted SARS-CoV-2 (Bao et al., 2020; Gao et al., 2020; Golden et al., 2020; Gu et al., 2020; Hassan et al., 2020; Imai et al., 2020; Jiang et al., 2020; Kim et al., 2020; Richard et al., 2020; Rockx et al., 2020; Rogers et al., 2020; Shi et al., 2020; Sia et al., 2020; Sun et al., 2020;

Winkler et al., 2020; Yu J. et al., 2020). However, except for antibodies or vaccine candidates, there are very limited reports at present successfully confirming the reduction of SARS-CoV-2 viral load in these models by treatment with drug candidates (Park et al., 2020). At this time, however, proposing an additional treatment choice with significant antiviral evidences is urgently demanded to combat COVID-19. Interestingly, MFQ showed a synergistic effect combined with NFV, a replication inhibitor for SARS-associated coronavirus (Yamamoto et al., 2004; Ohashi et al., 2021; **Figure 4**). These data would prospect better clinical outcomes by combined drugs with different modes of action, as used with antiviral therapy against HIV and HCV (Shen et al., 2008; Koizumi et al., 2017). Given the inhibition of viral entry, MFQ is also expected for prophylactic use. Its long half-life of approximately 20 days is advantageous for achieving a long-lasting antiviral state by a single oral administration. Consequently, our analysis highlights the anti-SARS-CoV-2 potency of MFQ, of which efficacy is expected to be further evaluated in the future through *in vivo* or clinical testing.

DATA AVAILABILITY STATEMENT

The original contributions presented in the study are included in the article/**Supplementary Material**, further inquiries can be directed to the corresponding author/s.

AUTHOR CONTRIBUTIONS

KW designed the study, critically revised the manuscript, and supervised the project. KS screened compounds in the cell-based screen. KS and MY performed biological experiments. KS and KW wrote the manuscript. KS, MY, SI, YI, SF, HO, WS, TT, SA, KK, SI, YT, TS, MM, MT, TW, and KW analyzed and discussed the results.

FUNDING

ACKNOWLEDGMENTS

for strategic research areas for SA. The retrovirus-based pseudoparticle system and human hepatoma cell line, Huh-7 cells were kindly provided by Dr. Francois-Loic Cosset at the University of Lyon and Dr. Francis Chisari at The Scripps Research Institute, respectively.

SUPPLEMENTARY MATERIAL

The Supplementary Material for this article can be found online at: https://www.frontiersin.org/articles/10.3389/fmicb. 2021.651403/full#supplementary-material

REFERENCES

Al-Bari, M. A. (2015). Chloroquine analogues in drug discovery: New directions of uses, mechanisms of actions and toxic manifestations from malaria to multifarious diseases. *J. Antimicrob. Chemother* 70, 1608-1621. doi: 10.1093/jac/dkv018

Bao, L., Deng, W., Huang, B., Gao, H., Liu, J., Ren, L., et al. (2020). The pathogenicity of sars-cov-2 in hace2 transgenic mice. *Nature* 583, 830-833. doi: 10.1038/s41586-020-2312-y

Bartosch, B., Dubuisson, J., and Cosset, F. L. (2003). Infectious hepatitis c virus pseudo-particles containing functional e1-e2 envelope protein complexes. *J. Exp. Med.* 197, 633-642. doi: 10.1084/jem.20021756

Chhonker, Y S., Sleightholm RL., Li J., Oupický D., and Murry DJ. (2018). Simultaneous quantitation of hydroxychloroquine and its metabolites in mouse blood and tissues using LC–ESI–MS/MS: an application for pharmacokinetic studies. *J. Chromatogr. B* 1072: 320-327.

Cifuentes Kottkamp, A., De Jesus, E., Grande, R., Brown, J. A., Jacobs, A. R., Lim, J. K., et al. (2019). Atovaquone inhibits arbovirus replication through the depletion of intracellular nucleotides. *J. Virol.* 93:e00389-19. doi: 10.1128/jvi.00389-19

Corman, V. M., Landt, O., Kaiser, M., Molenkamp, R., Meijer, A., Chu, D. K. W., et al. (2020). Detection of 2019 novel coronavirus (2019-ncov) by real-time rt-pcr. *Eurosurveillance* 25:2000045. doi: 10.2807/1560-7917.Es.2020.25.3.2000045

Cortegiani, A., Ippolito, M., Ingoglia, G., Iozzo, P., Giarratano, A., and Einav, S. (2020). Update i. A systematic review on the efficacy and safety of chloroquine/hydroxychloroquine for covid-19. *J. Crit. Care* 59, 176-190. doi: 10.1016/j.jcrc.2020.06.019

Desjardins, R. E., Pamplin, C. L., 3rd, von Bredow, J., Barry, K. G., and Canfield, C. J. (1979). Kinetics of a new antimalarial, mefloquine. *Clin. Pharmacol. Ther.* 26, 372-379. doi: 10.1002/cpt1979263372

DeWald, L. E., Johnson, J. C., Gerhardt, D. M., Torzewski, L. M., Postnikova, E., Honko, A. N., et al. (2019). *In vivo* activity of amodiaquine against ebola virus infection. *Sci. Rep.* 9:20199. doi: 10.1038/s41598-019-56481-0

Fan, H. H., Wang, L. Q., Liu, W. L., An, X. P., Liu, Z. D., He, X. Q., et al. (2020). Repurposing of clinically approved drugs for treatment of coronavirus disease 2019 in a 2019-novel coronavirus-related coronavirus model. *Chin. Med. J. (Engl).* 133, 1051-1056. doi: 10.1097/CM9.0000000000000797

Fukushi, S., Mizutani, T., Saijo, M., Matsuyama, S., Miyajima, N., Taguchi, F., et al. (2005). Vesicular stomatitis virus pseudotyped with severe acute respiratory syndrome coronavirus spike protein. *J. Gen. Virol.* 86, 2269-2274. doi: 10.1099/vir.0.80955-0

Funnell, S. G. P., Dowling, W. E., Muñoz-Fontela, C., Gsell, P. S., Ingber, D. E., Hamilton, G. A., et al. (2020). Emerging preclinical evidence does not support broad use of hydroxychloroquine in covid-19 patients. *Nat. Commun.* 11:4253. doi: 10.1038/s41467-020-17907-w

Gao, Q., Bao, L., Mao, H., Wang, L., Xu, K., Yang, M., et al. (2020). Development of an inactivated vaccine candidate for sars-cov-2. *Science* 369, 77-81. doi: 10.1126/science.abc1932

Geleris, J., Sun, Y., Platt, J., Zucker, J., Baldwin, M., Hripcsak, G., et al. (2020). Observational study of hydroxychloroquine in hospitalized patients with covid-19. *N. Engl. J. Med.* 382, 2411-2418. doi: 10.1056/NEJMoa2012410

Gendrot, M., Andreani, J., Boxberger, M., Jardot, P., Fonta, I., Le Bideau, M., et al. (2020). Antimalarial drugs inhibit the replication of sars-cov-2: An in vitro evaluation. *Travel Med. Infect Dis.* 37, 101873. doi: 10.1016/j.tmaid.2020.101873

Ghose, A. K., and Crippen, G. M. (1987). Atomic physicochemical parameters for three-dimensional-structure-directed quantitative structure-activity relationships. 2. Modeling dispersive and hydrophobic interactions. *J. Chem. Inf. Comput. Sci.* 27, 21-35. doi: 10.1021/ci00053a005

Golden, J. W., Cline, C. R., Zeng, X., Garrison, A. R., Carey, B. D., Mucker, E. M., et al. (2020). Human angiotensin-converting enzyme 2 transgenic mice infected with sars-cov-2 develop severe and fatal respiratory disease. *JCI Insight* 5:e142032. doi: 10.1172/jci.insight.142032

Gu, H., Chen, Q., Yang, G., He, L., Fan, H., Deng, Y. Q., et al. (2020). Adaptation of sars-cov-2 in balb/c mice for testing vaccine efficacy. *Science* 369, 1603-1607. doi: 10.1126/science.abc4730

Hassan, A. O., Case, J. B., Winkler, E. S., Thackray, L. B., Kafai, N. M., Bailey, A. L., et al. (2020). A sars-cov-2 infection model in mice demonstrates protection by neutralizing antibodies. *Cell* 182, 744-753.e4. doi: 10.1016/j.cell.2020.06.011

Hattori, S. I., Higshi-Kuwata, N., Raghavaiah, J., Das, D., Bulut, H., Davis, D. A., et al. (2020). Grl-0920, an indole chloropyridinyl ester, completely blocks sars-cov-2 infection. *mBio* 11:e01833-20. doi: 10.1128/mBio.01833-20

Hoffmann, M., Kleine-Weber, H., Schroeder, S., Krüger, N., Herrler, T., Erichsen, S., et al. (2020). Sars-cov-2 cell entry depends on ace2 and tmprss2 and is blocked by a clinically proven protease inhibitor. *Cell* 181, 271-280.e8. doi: 10.1016/j.cell.2020.02.052

Hu, J., Gao, Q., He, C., Huang, A., Tang, N., and Wang, K. (2020). Development of cell-based pseudovirus entry assay to identify potential viral entry inhibitors and neutralizing antibodies against sars-cov-2. *Genes Dis.* 7, 551-557. doi: 10.1016/j.gendis.2020.07.006

Imai, M., Iwatsuki-Horimoto, K., Hatta, M., Loeber, S., Halfmann, P. J., Nakajima, N., et al. (2020). Syrian hamsters as a small animal model for sars-cov-2 infection and countermeasure development. *Proc. Natl. Acad. Sci. U.S.A.* 117, 16587-16595. doi: 10.1073/pnas.2009799117

Jeon, S., Ko, M., Lee, J., Choi, I., Byun, S. Y., Park, S., et al. (2020). Identification of antiviral drug candidates against sars-cov-2 from fda-approved drugs. *Antimicrob. Agents Chemother* 64:e819-e820. doi: 10.1128/aac.00819-20

Jiang, R. D., Liu, M. Q., Chen, Y., Shan, C., Zhou, Y. W., Shen, X. R., et al. (2020). Pathogenesis of sars-cov-2 in transgenic mice expressing human angiotensin-converting enzyme 2. *Cell* 182, 50-58.e8. doi: 10.1016/j.cell.2020.05.027

Jones, R., Kunsman, G., Levine, B., Smith, M., and Stahl, C. (1994). Mefloquine distribution in postmortem cases. *Forensic. Sci. Int.* 68, 29-32. doi: 10.1016/0379-0738(94)90376-x

Karbwang, J., and White, N. J. (1990). Clinical pharmacokinetics of mefloquine. *Clin. Pharmacokinet* 19, 264-279. doi: 10.2165/00003088-199019040-00002

Keyaerts, E., Li, S., Vijgen, L., Rysman, E., Verbeeck, J., Van Ranst, M., et al. (2009). Antiviral activity of chloroquine against human coronavirus oc43 infection in newborn mice. *Antimicrob. Agents Chemother* 53, 3416-3421. doi: 10.1128/aac.01509-08

Kim, Y. I., Kim, S. G., Kim, S. M., Kim, E. H., Park, S. J., Yu, K. M., et al. (2020). Infection and rapid transmission of sars-cov-2 in ferrets. *Cell Host Microbe* 27, 704-709.e2. doi: 10.1016/j.chom.2020.03.023

Ko, M., Chang, S. Y., Byun, S. Y., Choi, I., d'Alexandry d'Orengiani, A.-L. P. H., Shum, D., et al. (2020). Screening of FDA-approved drugs using a MERS-CoV clinical isolate from South Korea identifies potential therapeutic options for COVID-19. *bioRxiv* [Preprint]. doi: 10.1101/2020.02.25.965582

Koizumi, Y., Ohashi, H., Nakajima, S., Tanaka, Y., Wakita, T., Perelson, A. S., et al. (2017). Quantifying antiviral activity optimizes drug combinations against hepatitis c virus infection. *Proc. Natl. Acad. Sci. U.S.A.* 114, 1922-1927. doi: 10.1073/pnas.1610197114

Lebeau, G., Vagner, D., Frumence, É., Ah-Pine, F., Guillot, X., Nobécourt, E., et al. (2020). Deciphering sars-cov-2 virologic and immunologic features. *Int. J. Mol. Sci.* 21:5932. doi: 10.3390/ijms21165932

Lim HS., Im JS., Cho JY., Bae KS., Klein TA., Yeom JS., et al. (2009). Pharmacokinetics of hydroxychloroquine and its clinical implications in chemoprophylaxis against malaria caused by Plasmodium vivax. *Antimicrob. Agents Chemother.* 534: 1468-1475.

Liu, J., Cao, R., Xu, M., Wang, X., Zhang, H., Hu, H., et al. (2020). Hydroxychloroquine, a less toxic derivative of chloroquine, is effective in inhibiting sars-cov-2 infection *in vitro*. *Cell Discov.* 6:16. doi: 10.1038/s41421-020-0156-0

Mastrangelo, E., Pezzullo, M., De Burghgraeve, T., Kaptein, S., Pastorino, B., Dallmeier, K., et al. (2012). Ivermectin is a potent inhibitor of flavivirus replication specifically targeting ns3 helicase activity: New prospects for an old drug. *J. Antimicrob. Chemother.* 67, 1884-1894. doi: 10.1093/jac/dks147

Matsuyama, S., Nao, N., Shirato, K., Kawase, M., Saito, S., Takayama, I., et al. (2020). Enhanced isolation of sars-cov-2 by tmprss2-expressing cells. *Proc. Natl. Acad. Sci. U.S.A.* 117, 7001-7003. doi: 10.1073/pnas.2002589117

McLachlan, A. J., Tett, S. E., Cutler, D. J., and Day, R. O. (1993). Absorption and in vivo dissolution of hydroxycholoroquine in fed subjects assessed using deconvolution techniques. *Br. J. Clin. Pharmacol.* 36, 405-411. doi: 10.1111/j.1365-2125.1993.tb00388.x

Mizutani, T., Fukushi, S., Saijo, M., Kurane, I., and Morikawa, S. (2004). Phosphorylation of p38 mapk and its downstream targets in sars coronavirus-infected cells. *Biochem. Biophys. Res. Commun.* 319, 1228-1234. doi: 10.1016/j.bbrc.2004.05.107

Nao, N., Sato, K., Yamagishi, J., Tahara, M., Nakatsu, Y., Seki, F., et al. (2019). Consensus and variations in cell line specificity among human metapneumovirus strains. *PLoS One* 14:e0215822. doi: 10.1371/journal.pone.0215822

Ohashi, H., Nishioka, K., Nakajima, S., Kim, S., Suzuki, R., Aizaki, H., et al. (2018). The aryl hydrocarbon receptor-cytochrome p450 1a1 pathway controls lipid accumulation and enhances the permissiveness for hepatitis c virus assembly. *J. Biol. Chem.* 293, 19559-19571. doi: 10.1074/jbc.RA118.005033

Ohashi, H., Watashi, K., Saso, W., Shionoya, K., Iwanami, S., Hirokawa, T., et al. (2021). Potential anti-COVID-19 agents, cepharanthine and nelfinavir, and their usage for combination treatment. *iScience.* 24:102367. doi: 10.1016/j.isci.2021.102367

Park, S. J., Yu, K. M., Kim, Y. I., Kim, S. M., Kim, E. H., Kim, S. G., et al. (2020). Antiviral efficacies of fda-approved drugs against sars-cov-2 infection in ferrets. *mBio* 11:e001114-20. doi: 10.1128/mBio.01114-20

Richard, M., Kok, A., de Meulder, D., Bestebroer, T. M., Lamers, M. M., Okba, N. M. A., et al. (2020). Sars-cov-2 is transmitted via contact and via the air between ferrets. *Nat. Commun.* 11:3496. doi: 10.1038/s41467-020-17367-2

Rockx, B., Kuiken, T., Herfst, S., Bestebroer, T., Lamers, M. M., Oude Munnink, B. B., et al. (2020). Comparative pathogenesis of covid-19, mers, and sars in a nonhuman primate model. *Science* 368, 1012-1015. doi: 10.1126/science.abb7314

Rogers, T. F., Zhao, F., Huang, D., Beutler, N., Burns, A., He, W. T., et al. (2020). Isolation of potent sars-cov-2 neutralizing antibodies and protection from disease in a small animal model. *Science* 369, 956-963. doi: 10.1126/science.abc7520

Rosenberg, E. S., Dufort, E. M., Udo, T., Wilberschied, L. A., Kumar, J., Tesoriero, J., et al. (2020). Association of treatment with hydroxychloroquine or azithromycin with in-hospital mortality in patients with covid-19 in New York state. *Jama* 323, 2493-2502. doi: 10.1001/jama.2020.8630

Shen, L., Peterson, S., Sedaghat, A. R., McMahon, M. A., Callender, M., Zhang, H., et al. (2008). Dose-response curve slope sets class-specific limits on inhibitory potential of anti-hiv drugs. *Nat. Med.* 14, 762-766. doi: 10.1038/nm1777

Shi, J., Wen, Z., Zhong, G., Yang, H., Wang, C., Huang, B., et al. (2020). Susceptibility of ferrets, cats, dogs, and other domesticated animals to sars-coronavirus 2. *Science* 368, 1016-1020. doi: 10.1126/science.abb7015

Sia, S. F., Yan, L. M., Chin, A. W. H., Fung, K., Choy, K. T., Wong, A. Y. L., et al. (2020). Pathogenesis and transmission of sars-cov-2 in golden hamsters. *Nature* 583, 834-838. doi: 10.1038/s41586-020-2342-5

Sinha, S., Medhi, B., and Sehgal, R. (2014). Challenges of drug-resistant malaria. *Parasite* 21:61. doi: 10.1051/parasite/2014059

Sun, J., Zhuang, Z., Zheng, J., Li, K., Wong, R. L., Liu, D., et al. (2020). Generation of a broadly useful model for covid-19 pathogenesis, vaccination, and treatment. *Cell* 182, 734-743.e5. doi: 10.1016/j.cell.2020.06.010

Suzuki, T., Itoh, Y., Sakai, Y., Saito, A., Okuzaki, D., Motooka, D., et al. (2020). Generation of human bronchial organoids for sars-cov-2 research. *bioRxiv* [Preprint]. doi: 10.1101/2020.05.25.115600

Tandon, R., Sharp, J. S., Zhang, F., Pomin, V. H., Ashpole, N. M., Mitra, D., et al. (2020). Effective inhibition of sars-cov-2 entry by heparin and enoxaparin derivatives. *J Virol.* 95:e01987-20. doi: 10.1128/jvi.01987-20

Tang, W., Cao, Z., Han, M., Wang, Z., Chen, J., Sun, W., et al. (2020). Hydroxychloroquine in patients with mainly mild to moderate coronavirus disease 2019: Open label, randomised controlled trial. *BMJ* 369:m1849. doi: 10.1136/bmj.m1849

Tani, H., Shiokawa, M., Kaname, Y., Kambara, H., Mori, Y., Abe, T., et al. (2010). Involvement of ceramide in the propagation of japanese encephalitis virus. *J. Virol.* 84, 2798-2807. doi: 10.1128/jvi.02499-09

Touret, F., Gilles, M., Barral, K., Nougairède, A., van Helden, J., Decroly, E., et al. (2020). In vitro screening of a fda approved chemical library reveals potential inhibitors of sars-cov-2 replication. *Sci. Rep.* 10:13093. doi: 10.1038/s41598-020-70143-6

Tree, J. A., Turnbull, J. E., Buttigieg, K. R., Elmore, M. J., Coombes, N., Hogwood, J., et al. (2020). Unfractionated heparin inhibits live wild-type sars-cov-2 cell infectivity at therapeutically relevant concentrations. *Br. J. Pharmacol.* 178, 626-635. doi: 10.1111/bph.15304

Wang, M., Cao, R., Zhang, L., Yang, X., Liu, J., Xu, M., et al. (2020). Remdesivir and chloroquine effectively inhibit the recently emerged novel coronavirus (2019-ncov) *in vitro*. *Cell Res.* 30, 269-271. doi: 10.1038/s41422-020-0282-0

Weston, S., Coleman, C. M., Haupt, R., Logue, J., Matthews, K., Li, Y., et al. (2020). Broad anti-coronavirus activity of food and drug administration-approved drugs against sars-cov-2 in vitro and sars-cov *in vivo*. *J. Virol.* 94:e01218-e20. doi: 10.1128/jvi.01218-20

Winkler, E. S., Bailey, A. L., Kafai, N. M., Nair, S., McCune, B. T., Yu, J., et al. (2020). Sars-cov-2 infection of human ace2-transgenic mice causes severe lung inflammation and impaired function. *Nat. Immunol.* 21, 1327-1335. doi: 10.1038/s41590-020-0778-2

Yamamoto, N., Yang, R., Yoshinaka, Y., Amari, S., Nakano, T., Cinatl, J., et al. (2004). Hiv protease inhibitor nelfinavir inhibits replication of sars-associated coronavirus. *Biochem. Biophys. Res. Commun.* 318, 719-725. doi: 10.1016/j.bbrc.2004.04.083

Yu, B., Li, C., Chen, P., Zhou, N., Wang, L., Li, J., et al. (2020). Low dose of hydroxychloroquine reduces fatality of critically ill patients with covid-19. *Sci. China Life Sci.* 63, 1515-1521. doi: 10.1007/s11427-020-1732-2

Yu, J., Tostanoski, L. H., Peter, L., Mercado, N. B., McMahan, K., Mahrokhian, S. H., et al. (2020). DNA vaccine protection against sars-cov-2 in rhesus macaques. *Science* 369, 806-811. doi: 10.1126/science.abc6284